NeuroImage 105 (2015) 525–535

Contents lists available at ScienceDirect

NeuroImage

journal homepage: www.elsevier.com/locate/ynimg

Functional connectivity dynamics: Modeling the switching behavior of the resting state

Enrique C.A. Hansen [a,1], Demian Battaglia [a,b,*,1], Andreas Spiegler [a], Gustavo Deco [c], Viktor K. Jirsa [a,*]

[a] Université Aix-Marseille, INSERM UMR 1106, Institut de Neurosciences des Systèmes, 27 Bd Jean Moulin, 13005 Marseille, France
[b] Bernstein Center for Computational Neuroscience, Am Faßberg 17, 37077 Göttingen, Germany
[c] Center for Brain and Cognition, Universitat Pompeu Fabra, Barcelona, Spain

ARTICLE INFO

Article history:
Accepted 3 November 2014
Available online 10 November 2014

Keywords:
Functional connectivity
Functional connectivity dynamics
Structural connectivity
Resting state
Brain dynamics
Whole brain computational model

ABSTRACT

Functional connectivity (FC) sheds light on the interactions between different brain regions. Besides basic research, it is clinically relevant for applications in Alzheimer's disease, schizophrenia, presurgical planning, epilepsy, and traumatic brain injury. Simulations of whole-brain mean-field computational models with realistic connectivity determined by tractography studies enable us to reproduce with accuracy aspects of average FC in the resting state. Most computational studies, however, did not address the prominent non-stationarity in resting state FC, which may result in large intra- and inter-subject variability and thus preclude an accurate individual predictability. Here we show that this non-stationarity reveals a rich structure, characterized by rapid transitions switching between a few discrete FC states. We also show that computational models optimized to fit time-averaged FC do not reproduce these spontaneous state transitions and, thus, are not qualitatively superior to simplified linear stochastic models, which account for the effects of structure alone. We then demonstrate that a slight enhancement of the non-linearity of the network nodes is sufficient to broaden the repertoire of possible network behaviors, leading to modes of fluctuations, reminiscent of some of the most frequently observed Resting State Networks. Because of the noise-driven exploration of this repertoire, the dynamics of FC qualitatively change now and display non-stationary switching similar to empirical resting state recordings (Functional Connectivity Dynamics (FCD)). Thus FCD bear promise to serve as a better biomarker of resting state neural activity and of its pathologic alterations.

Introduction

The complexity of human cognition is echoed in the dynamic organization of its accompanying brain signals. Even at rest, the brain does not remain in a state of equilibrium, but reveals complex spontaneous dynamics with intermittent spatiotemporal fluctuation patterns. In fact, functional magnetic resonance imaging (fMRI) studies have demonstrated that in the absence of an overt task, fluctuations in the blood oxygenation-level dependent (BOLD) fMRI signals correlate across functionally related brain regions in task conditions (Gusnard and Raichle, 2001; Laird et al., 2011; Raichle and Mintun, 2006). Further studies identified several intrinsic *resting state networks* (RSNs), which are found across subjects (Damoiseaux and Greicius, 2009), correlate with neuroelectric activity (Britz et al., 2010; Mantini et al., 2007) and are shaped, though not fully determined, by structural connectivity (SC) (Damoiseaux and Greicius, 2009).

Modeling studies (Deco et al., 2009; Deco et al. 2011; Ghosh et al., 2008; Honey et al., 2007) have demonstrated the importance of the interplay between anatomical structure, local neural dynamics and noise in the emergence of resting-state inter-regional correlations described by functional connectivity (FC) (Friston, 2011). Many of these models (Deco and Jirsa, 2012; Deco et al., 2013a; Ghosh et al., 2008) operate at a working point close to the critical edge of instability (Deco et al., 2013b). They are easily implemented within dedicated simulation environments such as The Virtual Brain (Sanz Leon et al., 2013) and are capable of reproducing time-averaged resting state FC. It has been pointed out, however, that purely statistical models, which predict FC on the basis of local and global descriptors of SC-weighted networks alone, are able to achieve a comparable or even closer fit (Goñi et al., 2014; Messé et al., 2014). This means that previous dynamic models went

Abbreviations: SC, structural connectivity; FC, functional connectivity; FCD, functional connectivity dynamics; MFM, mean-field model; LSM, linear stochastic model; eMFM, enhanced non-linearity mean-field model; RSN, resting state network; DSI, diffusion spectrum imaging; fMRI, functional magnetic resonance imaging; BOLD, blood oxygenation-level dependent.

* Corresponding authors at: Université Aix-Marseille, INSERM UMR 1106, Institut de Neurosciences des Systèmes, 27 Bd Jean Moulin, 13005 Marseille, France.
E-mail addresses: enrique-carlos.hansen@etu.univ-amu.fr (E.C.A. Hansen), demian.battaglia@univ-amu.fr (D. Battaglia), andreas.spiegler@univ-amu.fr (A. Spiegler), gustavo.deco@upf.edu (G. Deco), viktor.jirsa@univ-amu.fr (V.K. Jirsa).

[1] These authors contributed equally to this work.

http://dx.doi.org/10.1016/j.neuroimage.2014.11.001

scarcely beyond the exploration of how the SC skeleton expresses itself in spontaneous neural activity.

One drawback of all of these studies is that they assume —often implicitly— that FC is spatiotemporally stationary. In doing so, they ignore the profound non-stationarity of resting state activity (Hutchison et al., 2013). This activity possibly mirrors free thought modalities (Doucet et al., 2012) associated to neural activity events localized in space and time or to faster electrophysiological processes (Liu and Duyn, 2013), which are necessarily overlooked when averaging correlations throughout long recording periods. Thus models able to go beyond the mere replication of the constraints exerted by SC on FC are required to account for the time-dependence of FC.

Through simulations of computational models in a subcritical regime of activity, we show how the noise-driven exploration of a broad landscape of possible dynamical behaviors results in rapid switching between a discrete number of multistable FC states. This switching in turn gives rise to spatial correlation patterns reminiscent of known RSNs. Hence our approach offers a plausible interpretational framework for the non-stationarity of FC. In short, we propose that resting state Functional Connectivity Dynamics (FCD) are a manifestation of the self-organized activity of cortical networks, in which noise-driven fluctuations far from equilibrium lead to the stochastic sampling of a rich repertoire of characteristic system's trajectories.

Materials and methods

All empirical data used herein stem from a well-investigated data set as presented in Hagmann et al. (2008), comprising structural data from five healthy subjects and its associated time-series of resting state BOLD signals. In the following we organized the Materials and Methods into three subsections: on Connectivity, Mathematical Models, and Analyses.

Connectivity

Structural connectivity

Structural Connectivity is the set of anatomical connections between brain regions. Here we used the SC matrix of 66 regions derived from Diffusion Spectrum Imaging (DSI) as previously published and detailed in Hagmann et al. (2008) with the modifications introduced by Cabral et al. (2011), which made this matrix slightly asymmetrical. Connections in this SC matrix were defined within a standard parcellation scheme (Desikan et al., 2006) and averaged over five healthy subjects. Table S1 provides the names and abbreviations of these Regions Of Interest (ROIs). We analyzed the SC matrix using graph theoretical measures (Rubinov and Sporns, 2010), to assess correspondences with neural activity patterns. In particular, we calculated the *in-strength* of each network node, that is the sum of the weights of the incoming connections (the sum of all the entries in each row of the SC matrix) to determine the local topology of individual brain regions. A second approach called *s-core decomposition* (described in Hagmann et al. (2008)) provided insight into more global correlations between the in-strength of different nodes in the network. The s-core is a connected subnetwork in which nodes have an in-strength greater than or equal to *s*. We varied the value of *s* in the range [0, ŝ], where ŝ is the maximum value of all entries of the SC.

Functional connectivity

Functional Connectivity (FC) describes the connectedness of two brain regions by means of the covariance between their time series. From the BOLD signals, we extracted a FC matrix by calculating the Pearson (zero-lag) correlation between the BOLD signals of any two brain regions. In a *static* FC matrix, a single correlation value was computed for each pair of regions across the entire time-series of BOLD signals a 20-min session per subject. Furthermore, we estimated the *time-dependent* FC matrices. Each full-length BOLD signal of 20 min is split up into 570 segments of 60 seconds, overlapping by 58 seconds. For each segment, centered at time *t*, we calculated a separate FC matrix, FC*(t)*, thereby generating a stream of FC*(t)* matrices from each session. Similarities between different FC or FC*(t)* matrices were analyzed by plotting scatter plots of the upper triangular parts of two matrices and evaluating the Pearson correlation coefficient of these scatter plots. The static and time-dependent FC analysis was performed for the recordings of each subject as well as for each computational model based on time-series of 20 min of simulated BOLD signals (see below for details). The statistical significance of the differences between inter-FC correlation values (e.g. the correlations between empirical and simulated static FC matrices at the best-fit point of different models, defined below in the Results section) was tested using a resampling approach (1000 bootstrap replicas of each inter-matrix correlation, obtained by direct resampling with replacement of FC matrix entries).

Functional connectivity dynamics

To capture the spatiotemporal organization of functional connectivity, we derived a novel metric by representing the similarities between FC(t) matrices at different times t within a single matrix. We refer to this matrix as the *FC Dynamics (FCD) matrix*. The (t_1, t_2) entry of the FCD matrix provided the Pearson correlation between the upper triangular parts of the two matrices FC(t_1) and FC(t_2). Blocks of elevated inter-FC(t) correlations organized around the FCD matrix diagonal denoted epochs of stable FC configurations. The boundaries between such blocks were determined by unsupervised clustering of the FC*(t)* (with the features for clustering provided by their upper triangular parts), using the K-means method (Hartigan and Wong, 1979). Selecting $K = 4$ was sufficient for capturing all the visible blocks and thus thereby separating prominent epochs of stability. Then we operationally defined a *FC state* as a cluster of similar FC(t) matrices, typified by the cluster-average FC matrix.

Please note that our FCD analysis is similar to the meta-recurrence plots first described in (Manuca and Savit, 1996), constructed by comparing different chunks of the signals themselves, rather than their correlation matrices. We also computed meta-recurrence plots of activity, based on vectors of BOLD signals averaged for the different regions over the same time-windows used for a parallel FCD analysis. Please note that we retained the BOLD baselines in the signals and computed the cross-correlation (not the cross-covariance) between spatial patterns of window-averaged activity.

Mathematical models

Here we present three computational models of resting state network dynamics: a mean field model (MFM), previously introduced in Deco et al. (2013a); a simple linear stochastic model (LSM), already considered in (Galan, 2008; Goñi et al., 2014; Messé et al., 2014); and, finally, a minimally modified variant of the MFM, in which local non-linearities are enhanced to introduce bi-stability between a high and low firing rate states (eMFM) at the level of each single brain region.

Dynamical mean-field models (MFM and eMFM)

We used a modified version of the mean-field model designed by Wong and Wang (2006), to describe the mean neural activity for each brain region, following the reduction performed in Deco et al. (2013a). The resulting neural mass equations are given by:

$$\frac{dS_i}{dt} = \frac{-S_i}{\tau_S} + (1-S_i)\gamma R_i + \sigma\eta_i(t) \tag{1}$$

$$R_i = \frac{ax_i - b}{1 - exp[-d(ax_i - b)]} \tag{2}$$

$$x_i = wJ_N S_i + J_N G \sum_j C_{ij} S_j + I_0 \tag{3}$$

where S_i represents NMDA synaptic input currents and τ_S the NMDA decay time constant; R_i are collective firing rates; $\gamma = 0.641$ is a kinetic parameter; $a = 270(\mathrm{V}\cdot\mathrm{nC})^{-1}$, $b = 108$ Hz, and $d = 0.154$ s are parameters values for the input–output function; x_i are the total synaptic inputs to a region; $J_N = 0.2609$ nA is an intensity scale for synaptic currents; w is the relative strength of recurrent connections within the region; and C_{ij} are the entries of the SC matrix globally reweighted by a single scalar G adjusted as a control parameter; σ is the noise amplitude; and η is a stochastic Gaussian variable with a zero mean and unit variance. Finally, I_0 represents the external input and sets the level of regional excitability. Different sets of parameters yield different neural network dynamics and patterns of FC non-stationarity. In the model from Deco et al. (2013a), denoted herein simply as the *mean-field model* (MFM), we used $G = 2.4$, $\sigma = 0.001$, $w = 0.9$, $I_0 = 0.3$ nA. Analyses of the MFM model are presented in Figs. 1D-E, 2D, 3C, S3A-B and S5A (as indicated by a corresponding graphical cartoon, with dark blue balls connected by a wireframe connectivity skeleton). We also considered a minimal variant of the MFM, denoted herein as the *enhanced non-linearity mean-field model* (eMFM), which shares actually the same dynamical equations with the MFM, but adopting slightly modified parameters. We used, notably, $G = 1.2$, $\sigma = 0.006$, w = 1.0, $I_0 = 0.32$ nA.

The linear stochastic model (LSM)

We also considered a third simplified model in which no neural mass dynamics were adopted. The neural activity of each brain region was provided by a linear stochastic model (Galan, 2008; Goñi et al., 2014; Messé et al., 2014), which can be written as follows:

$$\frac{dr_i}{dt} = -r_i(t) + G\sum_j C_{ij} r_j(t) + \sigma\eta_i(t) \tag{4}$$

where r_i are activities of different brain regions and, as before, G is a scalar used to rescale the weights C_{ij} of the connectivity matrix (i.e. the

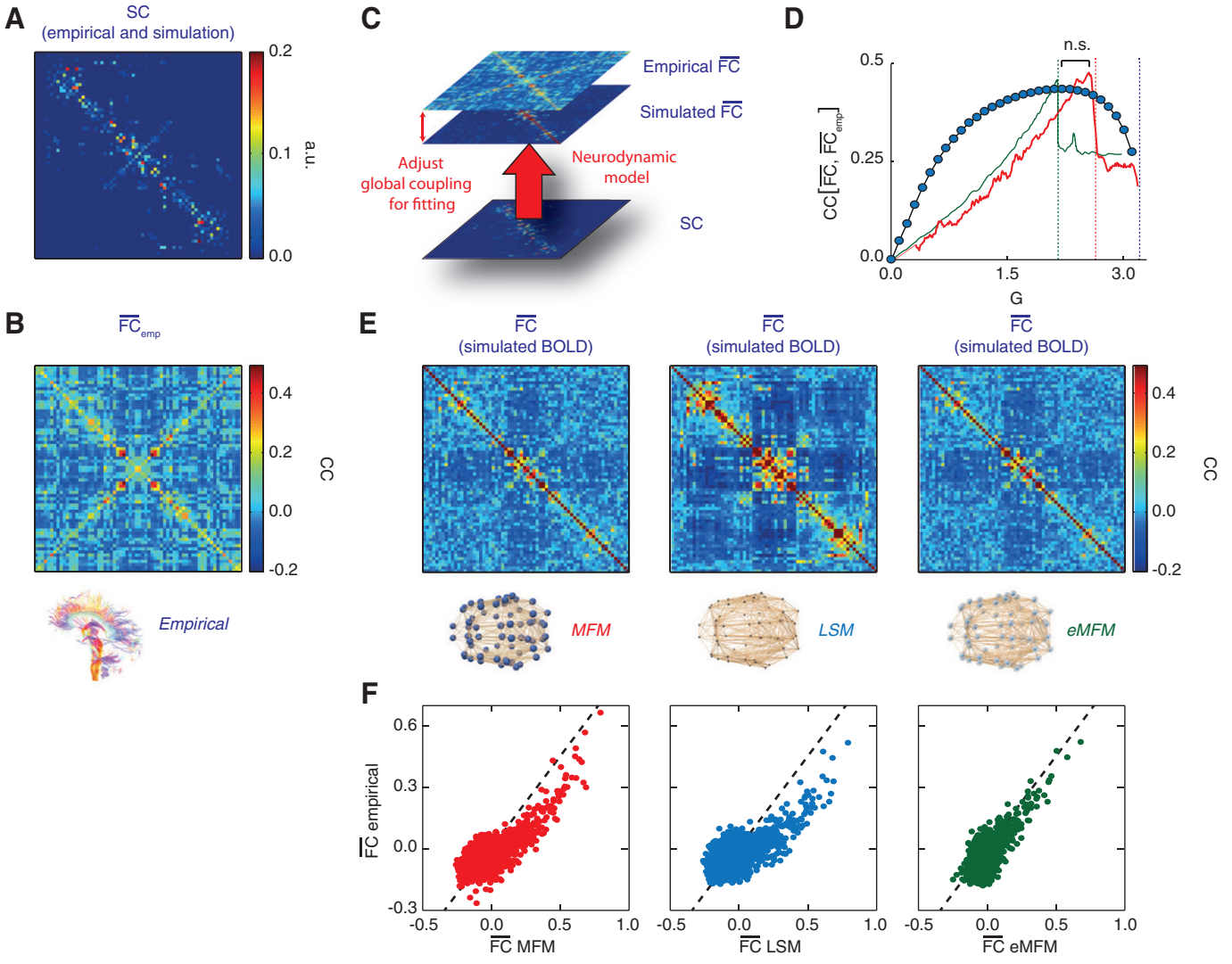

Fig. 1. Structure largely accounts for static FC. A: Structural Connectivity (SC) matrix estimated from averaged DSI analyses of human subjects (Hagmann et al., 2008). B: Empirical static Functional Connectivity (FC) matrix, averaged over 5 human subjects and estimated from 20 min of BOLD resting state recordings per subject (Hagmann et al., 2008). We consider three computational models of whole-brain dynamics: a mean-field model (MFM) from Deco et al. (2013a); a linear stochastic model, and a mean-field model with enhanced non-linearity (eMFM). Specific pointer icons designate analyses of the MFM, the LSM and the eMFM (and of empirical data). C: in all three models we adopt the SC matrix in panel A. A single global coupling parameter G is adjusted to optimize the overlap between the simulated static FC ($\overline{FC}$) and the empirical static FC ($\overline{FC_{emp}}$) shown in panel B. D: correlation between $\overline{FC_{emp}}$ and the simulated $\overline{FC}$ for each of the three models: MFM (left), the LSM (middle) and the eMFM (right). When tuning the coupling strength G, peak correlations from the LSM did not differ significantly from the best fit achieved by the MFM or the eMFM. Dashed vertical lines indicate critical instability points (color code corresponding to the model). E: simulated static FC from the MFM (left), LSM (middle) and eMFM (left), tuned at their best-fit point (cf. panel D) and with low noise ($\sigma = 0.001$). F: scatter plots of empirical and best-fit simulated BOLD inter-regional pairwise correlations. The 66 rows and columns of all SC and FC matrices shown above are given: first for the right hemisphere brain regions (order listed in Table S1); and then for the left hemisphere regions (reverse order, hence the anti-diagonal structure).

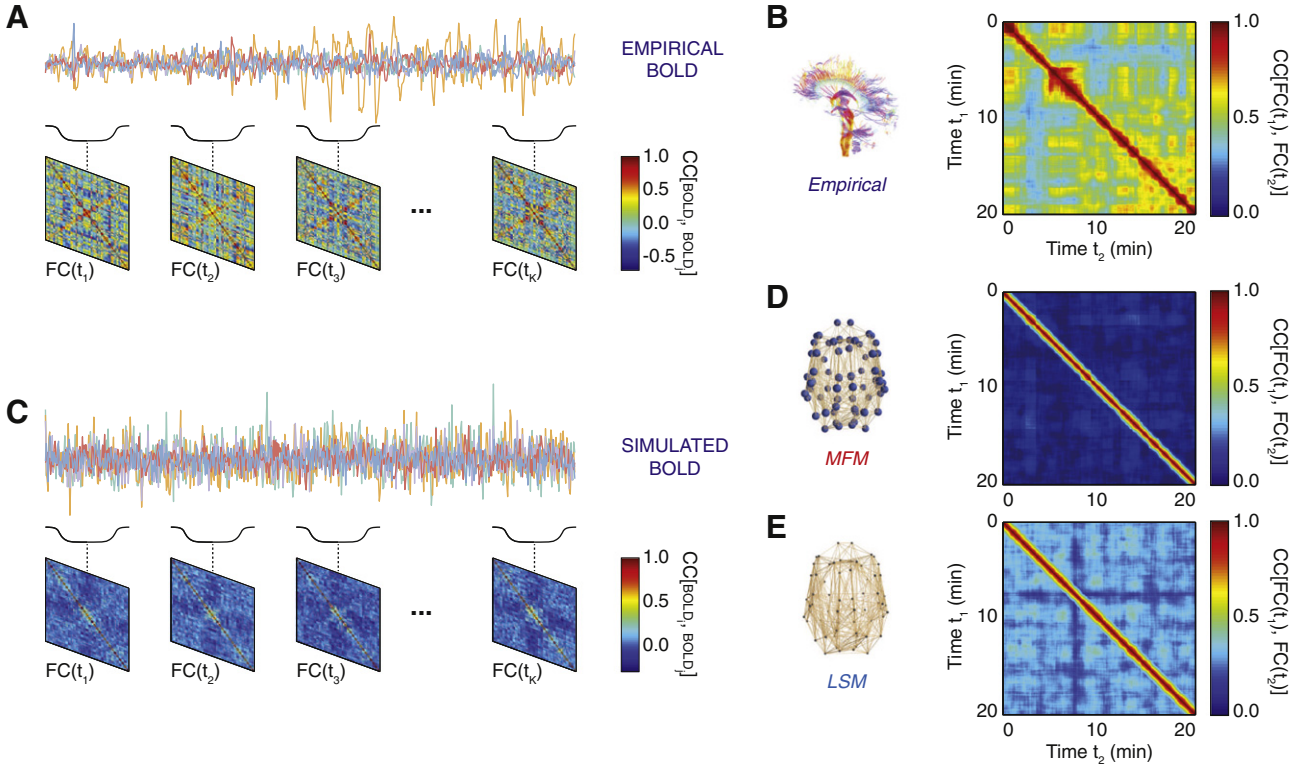

Fig. 2. Switching resting state functional connectivity is not captured by models optimized for static FC. A: as revealed by a time-windowed analysis (length of sliding window, 1 m), FC networks extracted from resting state BOLD signals (empirical data) evolve over time. B: a Functional Connectivity Dynamics analysis (FCD) of resting state empirical BOLD reveals the existence of fast switching transitions between different FC states. C: simulated BOLD signals generated by computational models optimized to fit static FC give rise to a trivial FC dynamics, which reveals lack of structured switching between FC states. D: a typical FCD matrix for the MFM. E: a typical FCD matrix for the LSM. For both the MFM and the LSM, simulations were performed at the respective static FC best-fit point.

same SC matrix as for the MFM and eMFM), σ is the noise amplitude and η_i are stochastic Gaussian variables with a zero mean and unit variance. This simple linear stochastic model (LSM) has, in the absence of noise, two different regimes. In the first regime, the activities of all regions converge to a fixed-point of zero activity, after an initial transient. In the second regime, regional activities diverge with exponential growth.

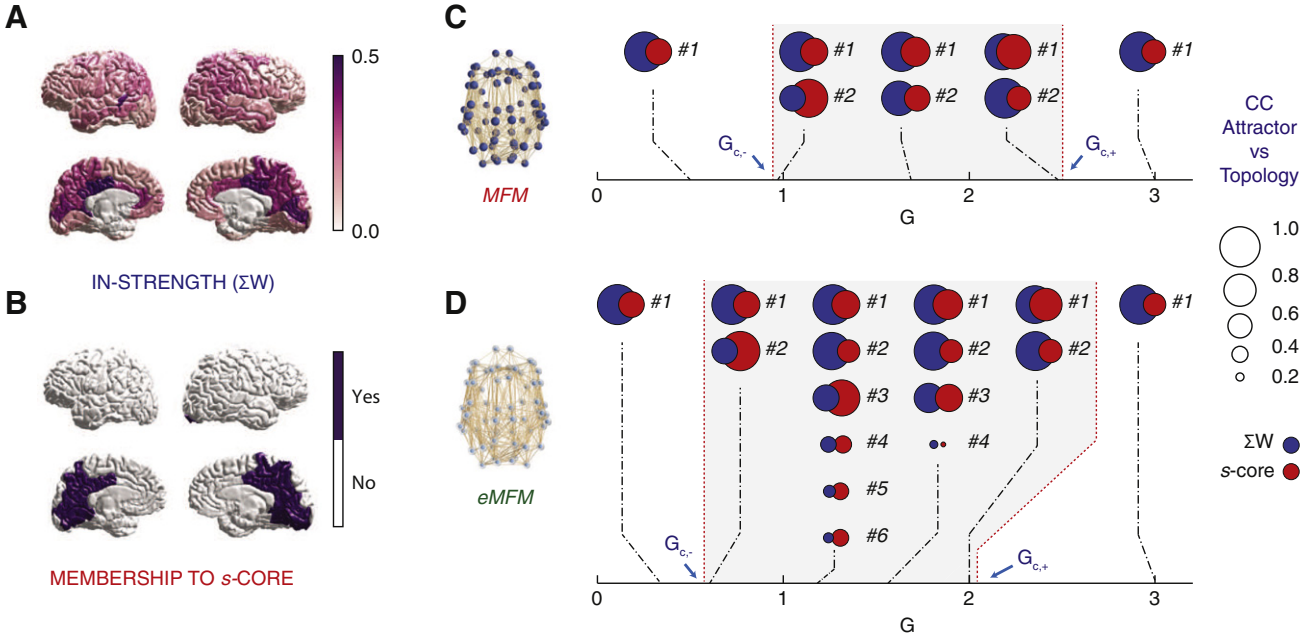

Fig. 3. A richer dynamical repertoire, beyond SC constraints. A: map of the heterogeneous SC in-strength of different brain regions. B: map of the brain regions belonging to the *s*-core of the SC network. C: the neural dynamics of MFM give rise to activation patterns strongly correlated either (blue circles) with the heterogeneous in-strengths of the different cortical nodes or (red circles) with the localization of the *s*-core of the SC network. D: By enhancing the non-linearity of the local neural mass dynamics, as in the eMFM model, a larger number of dynamical attractors appears in the critical range $G_{c-} < G < G_{c+}$ (shaded in gray). Some of these attractors (activation patterns) are poorly correlated with SC, which are a manifestation of self-organized collective dynamics. Labels in the figure (#1, #2…) enumerate classes of fixed points with different correlation values with the SC topology.

Therefore, we first searched for the range of values of G for which the system is stable, denoting as $\hat{G}$ the instability point. For each different G, the noise amplitude was then set to $\sigma = \hat{G} - G$.

Simulated BOLD signals

Simulated neural activity (i.e. the NMDA synaptic activations for the MFM and the eMFM; and the activations for the LSM) was converted into simulated BOLD signals, using a Balloon-Windkessel model (Friston et al., 2003). The resulting time-series were then downsampled at 2 s, as for empirical BOLD signals.

Computer simulations and fixed-point analysis

To systematically sample the repertoire of the fixed-point attractors of the dynamical models, we performed simulations without noise (deterministic evolution). For both the MFM and the eMFM, we varied G in the range $0 < G < 3.25$ with small increments of $\Delta = 0.05$. We performed 1000 simulations for each value of G using random initial conditions drawn from a uniform distribution over the entire range $0 < S_i < 1$. In the range $G_{c-} < G < G_{c+}$ characterized by network-level multistability, this wide diversity of initial conditions guaranteed an exhaustive sampling of both attractors with dominantly high activations and dominantly low activations (*high and low branches*). Consequently, we detected a broader range of G values leading to multistability with respect to previous studies (Deco et al., 2013a), and identified critical points with enhanced precision. Deterministic simulations were run for 15 seconds to achieve full equilibration and then the final fixed point was stored. In order to classify these fixed-point attractors, we computed correlations between their firing rate patterns and different topological features of SC, such as the in-degree or the binary membership to the s-core (choosing the largest value of s which did not lead to an empty core subgraph). The discreteness of the distributions of the correlations between attractors and topology allowed us to isolate distinct, well-defined classes of fixed points at each value of G by visual inspection.

In all stochastic simulations (for MFM, eMFM and LSM), we adopted a stochastic Euler integration method (Mannella, 2002) with a fixed integration step $dt = 0.1$ ms. We obtained similar results using $dt = 0.05$ ms.

Analyses: matching RSNs with simulated FC states

For six of the most common resting state networks (RSNs) reported by Mantini et al. (2007), we identified a short list of regions typically composing them, based on reported descriptions. This simple meta-analysis defined binary masks of the memberships of each brain region to each of the different RSNs (RSN1 to RSN6). In these masks the entry corresponding to a given brain region was set to one if this region was reported as belonging to a specific RSN, otherwise to zero. We then generated long, noise-driven simulations of resting state activity, with a noise level $\sigma = 0.006$, initializing the eMFM into different pre-stored attractors in the middle of the range $G_{c-} < G < G_{c+}$ (branches II–VII in Fig. S5B). From each of these simulated recordings, we extracted time-dependent FC(t) streams, computed the associated FCD matrices, and extracted prominent stable FC states using K-means unsupervised clustering (separately for each FC(t) stream), as previously described. We thus compiled a library of simulated FC states α, each of which was well represented by a corresponding representative FC matrix FC(α), obtained by averaging all the FC(t) belonging to the α cluster. We ran overall a total of 60 different resting state simulations (of 20 min). Each of these simulations contributed four FC clusters, each of which provided a template matrix FC(α). Thus, our library included 240 putative FC states. Rows FC$(\alpha)_i$ of these FC(α) matrices corresponded to typical seed correlation networks of a given region i, mapping inter-regional correlations with an area i associated to a specific FC state α. For each RSN, we then performed an exhaustive search into our library for the seed correlation network FC$(\alpha)_i$ which was most closely correlated with the corresponding binary membership mask M_{RSN}. We thus searched for the best matched seed correlation network among a vast number of 14,844 (66 brain regions times 240 FC templates) possible matrix rows. The retrieved best match FC$(\alpha)_i$ are plotted in the right column of Fig. 5A (correlation values thresholded at CC > 0.3).

For comparison, we also generated an ensemble of empirical seed correlation networks. Ten different time-series of resting state BOLD recordings were obtained from five different subjects (for a total of 150 min), giving rise to 40 clusters of empirical FC(t) matrices, which were at our disposal. From their representatives FC(α), we were able to extract a second ensemble of 2,640 empirical seed correlation networks.

Finally, given the number of simulated and empirical seed correlation networks, large overlaps between FC$(\alpha)_i$ and RSN masks could have been expected to arise just by chance. To assess the significance of the overlap achieved by the eMFM, we constructed a third ensemble of randomized seed correlation networks (null hypothesis). First, we randomly selected a FC(α) matrix within the 240 matrices available in the eMFM-derived library; then, we performed a random permutation of the columns of this matrix, maintaining the total functional out-strength but not the in-strength of each brain area. A randomly selected row of this scrambled functional connectivity template provided a seed connectivity network for the randomized ensemble. This list of steps was replicated 14,844 times to build a randomized ensemble of seed correlation networks, which was the same size as the eMFM-derived library. For each given ensemble of seed correlation networks (eMFM, empirical BOLD or randomized), we computed correlations with each RSN mask, thereby deriving three distributions of overlaps for each RSN under consideration.

Results

The results are organized as follows: Fig. 1 illustrates the ability of the three considered models to account for static (time-averaged) resting state FC. Fig. 2 displays the rich FCD typical of empirical resting state BOLD data, and the failure of the MFM and the LSM to reproduce such FCD. Fig. 3 explores the repertoire of possible dynamical attractors of the MFM and of the eMFM, and relates these deterministic fixed-point patterns of neuronal activity to the underlying topology of SC. Fig. 4 illustrates the richer FCD manifested by the eMFM in a subcritical regime far away from rate instabilities. Finally, Fig. 5 shows the non-random inter-relation between simulated FCD and well-known Resting State Networks (RSNs).

SC largely accounts for stationary aspects of FC

Following Deco et al. (2013a), we used neural masses of the Wong-Wang type (Wong and Wang, 2006) to describe the neural activity of each different local region in a reference parcellation with 66 brain regions (Desikan et al., 2006; cf. Table S1). The MFM model was endowed with a realistic inter-regional SC, derived from DSI data (Hagmann et al., 2008) and represented in Fig. 1A. In most applications reported in the literature, parameters of the MFM were optimized to maximize the similarity between a time-averaged empirical static matrix (Fig. 1B), obtained by computing a unique inter-regional correlation matrix between resting-state BOLD time-series lasting 20 min, and a simulated static FC matrix , computed in an analogous way from synthetic BOLD signals derived from the model. Once the SC skeleton and the neural mass parameters were fixed, only the global strength of inter-areal coupling G remained adjustable as a control scale (Fig. 1C). The noise-driven dynamics of the resulting whole-brain network were then simulated for different values of G, generating neural activity time-series, which were further transformed into synthetic BOLD signals (see Materials and Methods). The correlation between simulated and empirical reached values as high as ~ 0.47 (95% c.i. [0.44, 0.49],

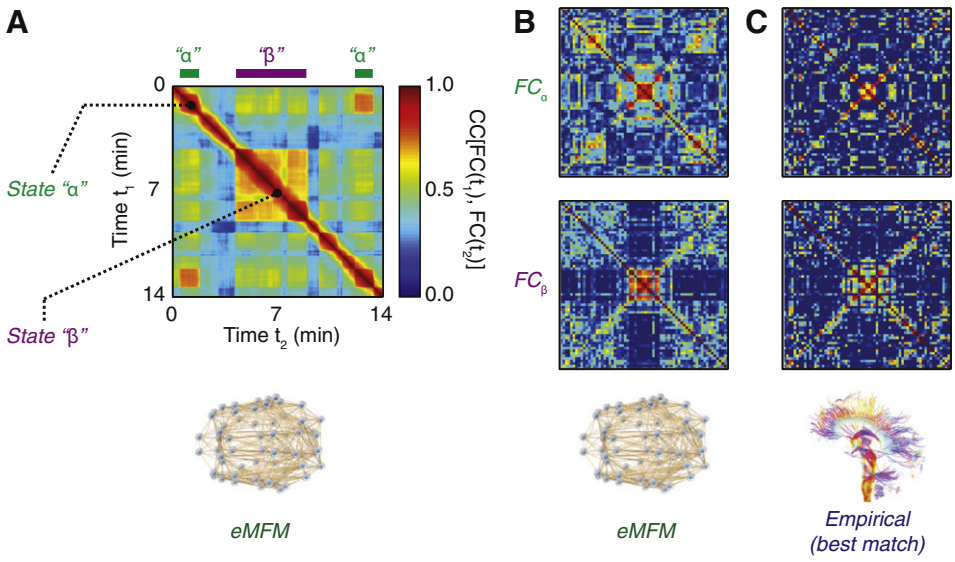

Fig. 4. A richer dynamical repertoire leads to FC switching. A: when selecting G in the middle of the critical range, the eMFM model develops a structured, out-of-equilibrium dynamics associated with self-organized switching between FC states. This is revealed by the block structure of the FCD matrix, which is comparable to that of empirical data (cf. Figs. 2B and S1), indicative of switching, in the selected time-interval, between two FC states labeled "α" and "β". Epochs of stability in these two FC states are also highlighted ("α" state epochs in green, "β" state epochs in violet). Further examples of switching FCDs, with other initial conditions in the range of $G_{c-} < G < G_{c+}$ can be seen in Fig. S6A. B: representative FC(t) matrices obtained from time windows within "α" state epochs (FC_α, top) or within "β" state epochs (FC_β, bottom). C: $FC(t)$ matrices extracted from empirical BOLD data and selected for their similarity to the simulated matrices FC_α and FC_β. Note that the FC matrices shown in panels B and C clearly deviate from the corresponding static FC, shown in Fig. 1B for empirical data and in Fig. 1E (right) for the eMFM.

Fig. 1D), growing with G to reach a maximum at a critical rate instability point G_{c+}, beyond which only a globally high firing rate state maintained its stability (Deco et al., 2013a,b; see below sections for more details).

The simulated static FC matrix $\overline{FC}$ obtained at the best-fit critical point of the MFM is shown in Fig. 1E. Here we explore its similarity with $\overline{FC_{emp}}$. It shows a scatter plot of individual inter-regional pairwise correlations generated by the MFM model (i.e. $\overline{FC}$ entries) against the corresponding entries. The shape of the cloud of points in this scatter plot indicates a linear correlation.

The non-random relation between empirical and simulated static FC is apparent even at visual inspection, if we compare the matrices in Figs. 1E and B. The most striking difference with $\overline{FC_{emp}}$ is that the functional couplings between homologous brain regions in different hemispheres (i.e. entries along the anti-diagonal of the static FC matrix) are under-represented in the $\overline{FC}$ from the MFM model (and also the LSM and the eMFM, see below). In computational models, this under-representation is indeed known to generate artifacts in the representation of all aspects of resting state FC (Messé et al., 2014). Although the fitting performance of the MFM was nontrivial, the correlation between the empirical static FC matrix and the SC matrix reached by itself a value of ~0.32 (95% c.i. [0.28, 0.36]). By evaluating the partial correlation between $\overline{FC}$ and $\overline{FC_{emp}}$, which was not accountable for by their common strong correlation with the SC matrix, we found a partial correlation of only ~0.21, which is still significantly above the null hypothesis expectations ($p < 0.001$, permutation testing), but considerably smaller. This suggests that the fitting performance achieved by the MFM could reflect more the use of a realistic structural connectivity, than an important role of MFM dynamics in shaping FC.

To gain additional insight into the relative relevance of structure and dynamics in explaining the actual performance of the MFM, we further simplified our whole-brain model. We ignored any non-linear aspects of the local dynamics within brain regions. Moreover, we assumed that the activity of a network node depends linearly on the total input from the neighboring nodes and on the incoming noise drive (see Materials and Methods). In this linear stochastic model (LSM) (Galan, 2008; Goñi et al., 2014; Messé et al., 2014), the fluctuations of local activations and their correlations among different sites are shaped only by the SC, and remain unchanged with respect to Deco and Jirsa (2012) and Deco et al. (2013a). By increasing G, stronger inter-node correlations developed. The resulting time-averaged correlation matrix $\overline{FC}$ was compared with the empirical static BOLD $\overline{FC_{emp}}$. As shown in Fig. 1D, the correlation with $\overline{FC_{emp}}$ initially increased with G up to a maximum of ~0.43 at a subcritical value of G (but no longer at the critical point, as was in the case of the MFM). For $G > G_C$ the fluctuations of the system escaped any constraints imposed by the connectivity skeleton, owing to the now too shallow landscape minima (Horsthemke and Lefever, 2006).

The best-fit matrix from the LSM is shown in Fig. 1E (middle column), together with a scatter plot of the simulated plotted against the empirical static pairwise functional couplings (Fig. 1F, middle column). The peak correlation value achieved by the LSM was very similar to the one achieved by the MFM and, eventually, the difference between them was not statistically significant (comparison of bootstrap 95% confidence intervals). Furthermore, the static $\overline{FC}$ matrices obtained from the two models were closely correlated (~0.8). The observed quality of the static $\overline{FC}$ fit was thus largely explained by the SC-induced correlations, expressed in the LSM, and regardless of the richer local dynamics adopted in the MFM.

Beyond static FC: resting state FC is switching

The assumption that FC is spatiotemporally stationary is only valid as a first approximation. This is illustrated by Fig. 2A, in which we performed a time-windowed analysis of long resting state BOLD recordings (empirical BOLD). In order to extract time-dependent FC, we computed different BOLD correlation matrices for different time-windows, centered at time t and lasting 60 s. Thus we obtained a temporal sequence of matrices FC(t), for each recording session. These FC(t) matrices can differ greatly from the empirical static FC (compare e.g. Fig. 1B with example FC(t)s in Fig. 4C).

We represented the rich structure of FC non-stationarity by means of a Functional Connectivity Dynamics (FCD) matrix (Fig. 2B). Each entry of the FCD matrix contains the value of the correlation between the

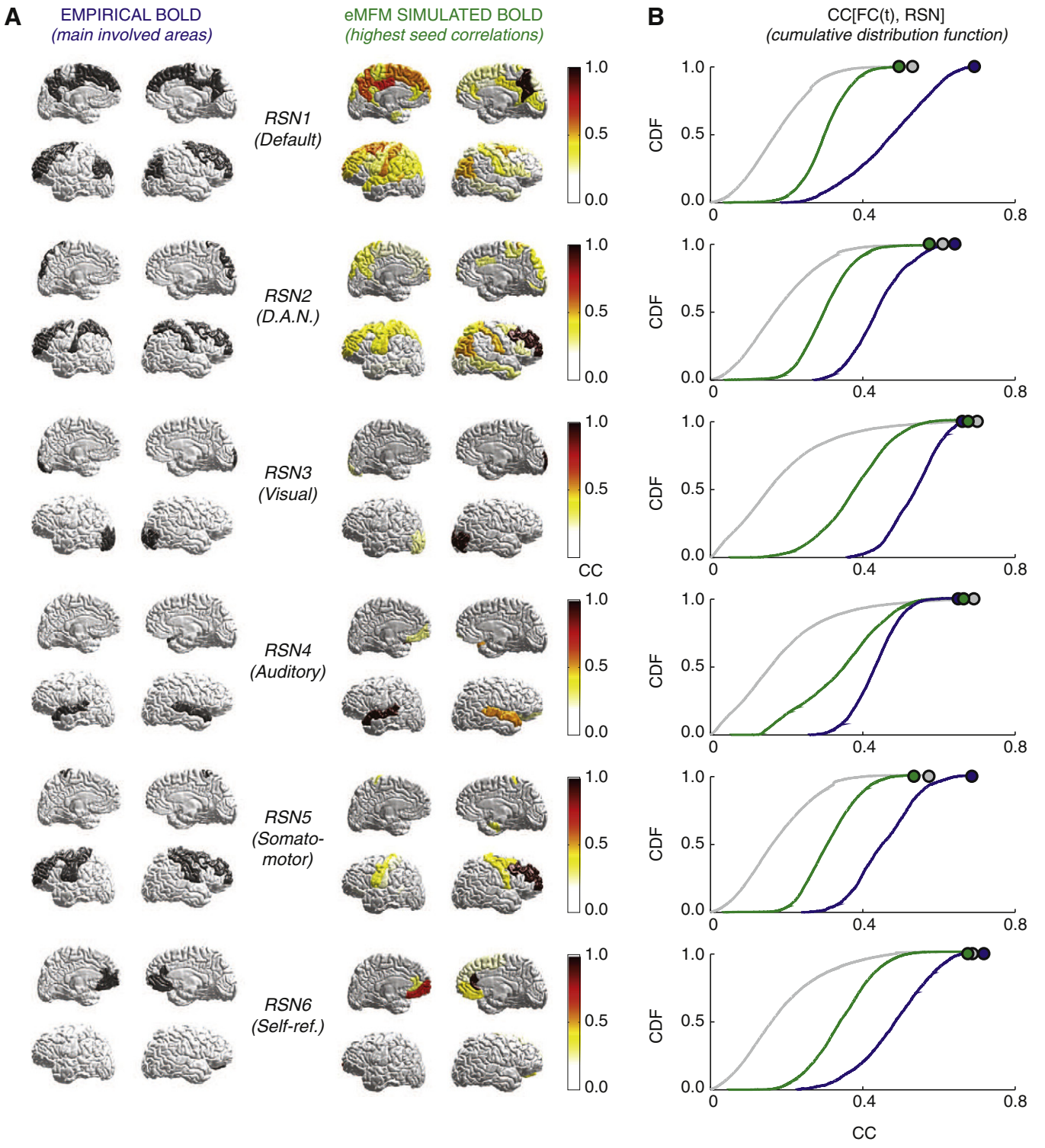

Fig. 5. The sampling of the dynamical repertoire of the eMFM reproduces Resting State Networks (RSNs). A: Seed correlation networks in selected (best-match) simulated FC states of the eMFM (right column) reveal a spatial structure reminiscent of typical RSNs (left column, where the main regions involved in a best-match RSN are plotted for comparison). The seed regions used were all in the right hemisphere. They were: precuneus (RSN1), rostral middle frontal (RSN2 and RSN5), lateral occipital (RSN3), superior temporal (RSN4), rostral anterior cingulate (RSN6). Plotted correlations are thresholded at 0.3. B: cumulative distribution functions (CDFs) of the distribution of overlaps between RSNs and time-dependent seed correlation networks extracted from empirical data (blue line) and eMFM simulations (green line). The CDF of the distribution of overlaps expected by chance is also shown for comparison (permutation testing, grey line). Colored filled circles indicate the maximum observed values of overlaps for each of the three equal-sized ensembles of seed correlation networks under consideration. If large overlaps with RSNs can also be accidentally observed for randomized ensembles of FC(t)s, significantly larger overlaps are generally observed for eMFM simulations, though still far from empirical data levels.

matrices FC(t_1) and FC(t_2) observed at times t_1 and t_2. FC(t)s were closely auto-correlated during epochs lasting several minutes, denoted in Fig. 2B by red, square-shaped blocks occurring along the diagonal. We used unsupervised clustering to precisely define the boundaries between these blocks, which were not always equally evident under visual inspection. Following the work of Allen et al. (2012), we identified

several clusters of FC(t), which we call *FC states*. Different FC states emerged over time, possibly reoccurring at different epochs within the same session. Transitions between FC states were often very sharp, associated to what we call a switching behavior. The FC(t) matrices remained often highly autocorrelated over minutes, and then suddenly (within one time-window) transformed into nearly uncorrelated FC patterns. Such epochs of stability were inter-twined with transients of instability, corresponding to a more gradual morphing of FC(t) matrices. FC substates (i.e. a finer clustering of FC(t) clusters found at a coarser timescale) may also exist, reminiscent of hierarchies of EEG microstates (Van De Ville et al., 2010). Additional FCDs from empirical BOLD data from other subjects can be seen in Fig. S1. Furthermore, FCDs for two other window sizes are shown for comparison in Fig. S2.

Please note that the FCD is positive defined, which is mathematically not a necessity. The FCD indicates the tendency of inter-areal couplings to change their intensity throughout the spontaneous evolution of resting state FC, but not their sign of FC. In other words, the number of correlated pairs which are transformed into anti-correlated pairs is limited.

Beyond SC: dynamics

Switching, although prominent in empirical FC, was not clearly visible in the simulated time-series of BOLD generated by computational models optimized to fit static FC, such as the MFM or the LSM. Despite the elevated correlations reached between the simulated and empirical static FCs, shown in Fig. 1E-F, major discrepancies appeared under a time-windowed analysis. The variability of simulated FC(t) displayed by the MFM — at least at a working point optimized to best fit static FC — was in fact quite unstructured, as is shown by the associated FCD matrix in Fig. 2D. Analogously, Fig. 2E shows a typical FCD matrix for the LSM, which is qualitatively similar to that of Fig. 2D. Darker colored stripes are visible in the FCD of the LSM in Fig. 2E. These stripes highlight specific events in which FC*(t)* is anomalously reorganized with respect to the FC*(t)* matrices observed at other time instants. However, in both the MFM and the LSM, FC(t) pairs separated by longer time-lapses than the adopted sliding window are generally poorly correlated, and there are no long-lasting epochs in which FC(t) transiently stabilizes, in marked contrast with empirical FCD (at all the tested noise levels, cf. Fig. S3).

To explore the nature of the time dependency of FC in more detail, we correlated the activity profiles of the simulations with different descriptors of SC topology, including the in-strengths (Fig. 3A) and the *s*-core (Fig. 3B). While the total in-strength is a descriptor of local topology and depends only on incoming connections to each given area, membership to the *s*-core captures the global aspects of SC (see Materials and Methods). As illustrated in Fig. 3C, the activity profiles associated with the MFM fixed points over the entire wide range of G that we explored were always closely correlated with local and global SC topology. For $G < G_{c-}$ or for $G > G_{c+}$, only one fixed point existed. Even if the average activity level was higher for the second interval of stronger coupling, in both cases, variations of activity between different brain regions reproduced the changes in the relative in-strength (correlation values plotted as blue circles). In the intermediate range of $G_{c-} < G < G_{c+}$, the dynamic repertoire was enriched, as reported in Deco and Jirsa (2012) and Deco et al. (2013a). However, when considering the relationships to the underlying SC topology, all the sampled fixed points appeared to fall simply into two categories: one in which strong correlations with local topology continued to subsist (Fig. 3C, correlation values plotted as blue circles), and another in which strongly activated brain regions tended to be restricted to the *s*-core (Fig. 3C). Thus the simulated dynamics of the MFM mirrored local and global SC topological aspects and provided little additional information.

To locally enhance the nonlinear dynamic nature of each network node, we modified the neural mass parameters adopted in the MFM, endowing each individual brain area in isolation with a bistability between a high and low level of activity (see Fig. S4). We thereby obtained a model that we denote as *enhanced non-linearity* MFM, or eMFM for short (see Materials and Methods). This local multi-stability reinforced the global emergence of the multi-stability already occurring in the MFM (Fig. 3C), by boosting its dynamical repertoire, beyond the constraints exerted by SC. As is evident from the comparison between the MFM (Fig. 3C) and the eMFM (Fig. 3D), additional classes of fixed points emerged in the range of $G_{c-} < G < G_{c+}$, with some of the associated activity profiles displaying now poor correlations with both local and global SC topology (cf. also Fig. S5 for a more detailed representation of the attractor landscape of the MFM and of the eMFM). The emergence of these classes of fixed points requires an interplay between local and collective dynamics and cannot be explained by SC alone, unlike the situation in Fig. 3C. We also note that, for the eMFM, the multi-stability range of $G_{c-} < G < G_{c+}$ is narrower and has shifted toward smaller values with respect to the MFM. This earlier stabilization of the high firing rate network states and destabilization of the low firing rate network states can be explained by the enhanced excitability of the eMFM neural mass, which is able to locally sustain a high firing rate state, without the need for steadily increasing any excitatory inputs from neighboring regions.

The sampling of the dynamical repertoire leads to FC switching

We expected more complex fluctuation patterns —and, potentially, a switching non-stationarity of FC(t)— to correspond to the richer repertoire of noiseless neural activity attractors of the eMFM (Fig. 3D) with respect to the MFM (Fig. 3C). We then performed noise-driven simulations of the eMFM model, adopting an increased noise level to achieve a more complete exploration of possible trajectories in phase space (see Fig. S3 for the effects of noise), and computed the associated BOLD time-series and subsequent FCD analysis. Fig. 4A illustrates a representative FCD matrix providing with an example of the FC*(t)* evolution resulting when the system is initialized at a *subcritical* value of G in the center of the range of $G_{c-} < G < G_{c+}$ (i.e. such as to maximize the number of attractors). The FCD matrix in Fig. 4A bears a qualitative resemblance to the switching FCDs in the empirical BOLD data shown in Fig. 2B and Fig. S1. At least two FC states, denoted as "α" and "β", remain stable for epochs lasting from a few tens of seconds to several minutes. These epochs are highlighted in different colors above the FCD matrix, and form, in the selected time-interval a sequence "α" to "β" and back to "α". Representative FC*(t)* matrices from epochs in the "α" and "β" states are shown in Fig. 4B, together with the closest matches we could find for them among the empirical FC*(t)* matrices extracted from our data-set of resting state BOLD. The model also reproduced the transients of increased instability and corresponding accelerated evolution and reconfiguration of FC networks, which can be observed in the empirical FCD matrices of Figs. 2B and S1. Similar FCD matrices describing switching, waxing and waning FC patterns were obtained for other subcritical initial conditions and sufficiently high noise levels (see Fig. S6). Even the original MFM gave rise to structured non-stationarity patterns (although they were always less prominent than for the eMFM), when G was selected at the center of the range of $G_{c-} < G < G_{c+}$ and when noise was increased. For both models, switching was suppressed when the noise level was reduced, or when approaching the critical points G_{c-} or G_{c+}, which was due in all these cases to a poor dynamical repertoire. An analysis of the role of noise in shaping FC dynamics for both the MFM and the eMFM (as well as the LSM) is shown in Fig. S3.

Interestingly, the strong fluctuations of FC(t) revealed by the FCD analysis of eMFM simulations often occurred without a parallel remodeling of the underlying activation profile. In fact, the correlation between activation patterns at different moments in time remained very high even when the corresponding correlations between FC(t) matrices dropped to smaller values. This can be seen by comparing the recurrence plots of activation patterns shown in Fig. S7A (see

Materials and Methods) with the corresponding FCDs in Fig. S6A. A similar behavior was manifested in the empirical BOLD data (cf. Fig. 2B with Fig. S7B).

Finally, we note a greater ability of the eMFM to account for the dynamical aspects of resting-state FC with a similar ability to account for the static aspects compared to the MFM. The best-fit simulated static generated by the eMFM is shown in Fig. 1E (right), together with a scatter plot of simulated vs. empirical pairwise functional couplings (Fig. 1F, right). For both the MFM and the eMFM, the best fit was achieved nearby their respective critical points. In neither of these two models, however, did this best fit regime lead to FC switching. On the contrary, FC switching was observed subcritically in the eMFM with respect to G_{c+} and at higher noise levels. Under these conditions, even the MFM displayed weak traces of emergent switching, although never as prominently as the eMFM (see Fig. S3B). In this subcritical regime, correlations between the simulated and empirical static FCs never exceeded 0.3. Nevertheless, correlations rose again to higher values when we considered the time-dependent functional connectivity patterns. Individual correlations between simulated FC(t)s and their best empirical match (extracted from the BOLD data at our disposal) reached, for the eMFM, a median value as high as ~ 0.6. Median best-match correlations were significantly higher in the eMFM than in the MFM ($p < 0.01$, Kruskal-Wallis). In fact, for all the tested noise values in the MFM (cf. Fig. S3), their median value never rose above ~0.4. Comparison at the distribution level, however, could not confirm the statistical significance of this difference ($p = 0.07$, two-way Kolmogorov-Smirnov).

The sampling of dynamical repertoire engenders RSN-like functional networks

Our model can retrieve FC states, which are reminiscent of well characterized RSNs. Fig. 5A shows the comparison between the main regions involved in the six RSNs reported by Mantini et al. (2007) (left column) and the spatial correlation maps engendered by different simulated FC states (right column). In searching for different RSNs, we extracted (through unsupervised clustering) a large library of FC states from long simulations of resting state activity. This library was generated from 60 different simulations, each lasting 20 min of real time. These simulations were initialized in the proximity of different attractors in the range $G_{c-} < G < G_{c+}$ (Figs. 3D and S5B), and included therefore an overall total of 240 FC(t) cluster templates (i.e. representative FC matrices of putative FC states). We then searched systematically for FC states and seed regions leading to the best match between the corresponding seed correlation networks and the different RSNs (see Materials and Methods). In Fig. 5A we identified related FC states for each of the six RSNs. The main regions involved in a given RSN (Fig. 5A, left) were typically highly correlated with the selected seed region in the correlation networks instantiated by the matching FC state (Fig. 5A, right). Our search procedure always selected seed regions distinctively associated with the matched RSN (Damoiseaux et al., 2006; Mantini et al., 2007), e.g. the precuneus for the RSN 1 (Default mode) or the rostral middle frontal cortex, for the RSN 2 (Dorsal Attentional Network). Nevertheless, in some cases, large simulated correlations also existed with regions not usually associated with the corresponding RSNs, e.g. between the precuneus and the post- and pre-central cortices for the Default Mode Network or between the rostral middle frontal and inferior parietal cortices for the Dorsal Attentional Network. Furthermore, it was not always possible to identify a clearly corresponding RSN (or known task-activated network) for each simulated FC state.

To verify the significance of our findings, we studied the statistical distributions of the overlaps between empirical RSNs and FC(t) networks from actual empirical resting state BOLD data and from synthetic BOLD generated by the eMFM in a subcritical high noise regime (as in Figs. 4A and 5A). Fig. 5B shows the cumulative distribution functions (CDFs) of the distribution of overlaps with each of the six RSNs under consideration with seed correlation networks retrieved in empirical data (blue), eMFM simulations (green) and streams of randomized FC(t) matrices (grey). Circles filled with corresponding colors indicate the largest RSN overlap values registered for each of the three distributions under consideration. For all the three ensembles and for all the RSNs, we found a broad range of possible overlaps. It was always possible to find overlaps between RSNs and randomized FC(t)s as high as those of the FC states from eMFM simulations. These chance-level overlaps were also commensurate with the overlaps found within the actual empirical FC(t) matrices. These maximum overlaps with empirical data rose above chance expectation only in the case of the Default Mode Network (RSN1) and of the Somatomotor Network (RSN5). This negative result concerns only the best-match cases, and means that it is finally not surprising to find matches as good as those in Fig. 5A between the RSNs and some isolated instance of FC(t) pinpointed in an extensive ensemble. However, the situation was completely different when we considered the entire distributions of observed overlaps. In this case, the CDFs of the RSN overlap distributions for the three considered ensembles were obviously different. In particular, RSN overlaps with randomized seed correlation networks were generally smaller than with the seed correlation networks observed in the eMFM simulations and in the empirical data ($p < 0.001$, Kolmogorov-Smirnov). Thus the sampling of FC states performed by the eMFM regularly gave rise to non trivial correspondences with known RSNs (and not just accidentally, as for randomized FC(t) streams). Nevertheless, these eMFM overlaps were significantly weaker than those for actual empirical data ($p < 0.001$, Kolmogorov-Smirnov).

Finally, the regional activation patterns corresponding to the seed correlation networks in Fig. 5A were less reminiscent of the matched RSNs and displayed a poorer variability (Fig. S8). This is in agreement with the previous observation that FC patterns can vary strongly in the virtual absence of variations of the spatial map of average activation (cf. Figs. S7 and Discussion).

Discussion

The non-stationarity of resting state connectivity imposes a paradigmatic shift in the way in which resting state functional interactions are analyzed (Hutchison et al., 2013) and simulated. Previous whole brain models, such as the MFM (Deco and Jirsa, 2012; Deco et al., 2013a), do not qualitatively reproduce the switching between FC states observed in empirical BOLD data (Fig. 2D). However, this failure is not due to the nature of the models themselves, but rather to the fact that, until now, the dynamic nature of these models had not been fully explored when considering regimes optimized to fit static FC best. Indeed, enabling a repertoire of possible dynamical modes richer than in the MFM was enough to instantiate FC state switching (Fig. 4). This finding legitimates our attempt to interpret resting state FC non-stationarity as an emergent hallmark of self-organized cortical dynamics.

By introducing multi-stability between high and low activity regimes at the level of single brain regions —a feature which is not unrealistic, but which could admit cognitively relevant interpretations, reflecting the possibility of sustained local activity such as in working memory (Miller et al., 2003) or decision making (Wong and Wang, 2006)— we emphasized non-linearity through a small parameter change and created dynamical attractors without any trivial relationship to local or global topology (Fig. 3D). In this way we reduced the strong constraints, which SC exerts on FC (Honey et al., 2007), and allowed mean-field dynamic simulations to behave in a qualitatively different way than that of purely structure-based models such as the LSM. It is important to stress, however, that the number of retrieved attracting firing rate patterns (six, in Figs. 3D and S5B) continued to be very small with respect to the exponentially large number of patterns of high and low firing rates (2^N) made possible, in principle, by local bistability at the level of each individual brain region. This means that SC continued to play a very important role in shaping the neural

dynamics of the eMFM, but that its role was no longer bound to induce a mirroring of SC strengths and cores.

The network system, in attempting to converge toward one of its fixed points, was maintained out-of-equilibrium by noise levels which were always higher than those adopted for the MFM in Deco and Jirsa (2012) and Deco et al. (2013a). Different subspaces were thus efficiently sampled along trajectories. These trajectories either converged back towards the fixed point from which they originated or escaped towards different attractors, thereby giving rise potentially to structured dynamic itinerancy (Bressler and Kelso, 2001; Rabinovich et al., 2008). Such out-of-equilibrium behaviors enlarge the already abundant repertoire of available fixed points in Fig. 3D. And this same dynamical repertoire —which was rich, yet, sufficiently stereotyped— enabled our model to generate metastable, reliably reproducible correlation patterns encompassing all the six RSNs reported by Mantini et al. (2007).

Our framework suggests that common RSNs are characteristic, high-dimensional fluctuation modes (or characteristic deviations from equilibrium trajectories) that are only indirectly related to fixed points of the deterministic network dynamics. As is evident in Fig. S8, in our simulations spatial maps of highly active regions did not necessarily correspond to the topography of the matching RSNs. As can be seen from the comparison between Figs. S6A and S7A, very different FC states could occur in our model in association with only slightly altered spatial patterns of activation. While activation patterns were dominated by static heterogeneities of baseline activity, the patterns of fluctuation around them were always highly dynamic and "liquid". In other words, FC states were not bound to mirror activation states. The fact that even empirical BOLD signals display a stronger variability of FC states than of activity patterns (compare Fig. 2B with Fig. S7B) constitutes an intriguing confirmation of a finding first initially predicted by our simulations.

We did not attempt a systematic mapping between RSNs and every possible subspace spanned by the dynamics of our enriched mean-field model (eMFM). We expect the same RSN to span multiple FC states. Analogously, a given FC state can generate fluctuation patterns related to multiple RSNs. We found that all the reference RSNs could be retrieved by initializing the system in the proximity of attractors arising in the entire range $G_{c-} < G < G_{c+}$, i.e. for working points which are *sub-critical* with respect to the critical point $G = G_{c+}$. We were, however, unable to identify a single critical value of G for which multi-stability between all the RSNs occurred simultaneously. This contrasts with previous studies, such as Deco et al. (2013a,b), which insisted on the importance of tuning the system precisely near the global rate instability occurring at $G = G_{c+}$, in analogy with critical neural avalanches (Beggs and Plenz, 2003). Still, inviting comparison with a Griffiths phase (Moretti and Muñoz, 2013), we can speak of a relatively narrow "critical range" of parameters, in which many bifurcations in cascade lead to the birth and death of a multitude of attractor branches, and result in the most entropic dynamical repertoire. Thus, in a sense, moving away from this rate instability makes the system even more critical. Similar conclusions were reached from different perspectives in Deco and Jirsa (2012) and Deco et al. (2012). Moreover, we observe that the phenomenon of FC switching was robustly manifested within the entire critical range, as indicated by Fig. S6A, reducing the necessity for a careful tuning of parameters or for mechanisms leading to self-organized criticality.

With the selected model parameters and without introducing delays in long-range connectivity, the deterministic behavior of both the MFM and the eMFM led only to fixed-point attractors (Figs. 3C-D). However, more elaborated models could also generate as well other types of behaviors, including the ultra-slow oscillations, known to characterize resting state dynamics (Deco et al., 2009; Ghosh et al., 2008) or chaotic behaviors (Honey et al., 2007). Here we chose to ignore oscillatory aspects as a first simplification step, limiting ourselves to verify that MFM and eMFM BOLD signals were spectrally similar (with most of the power concentrated over a broad band between 0 and 5 Hz, without no clear peaks) without attempting to fit of empirical BOLD spectra. Nevertheless, we expect that accounting for oscillatory states and out-of-equilibrium transients would further enrich the dynamical repertoire of our models, thereby reinforcing therefore the phenomenon of switching by further multiplying the classes of possible fluctuation patterns and FC states.

The general similarity between simulated FC(t)s and empirical RSNs is made apparent by the bulk distribution-level analysis in Fig. 5B, and even more than by the best-match cases represented in Fig. 5A. This phenomenon could have not been anticipated a priori, since our model was not intentionally designed to reproduce known RSNs and did not contain any *ad hoc* parameter tweak introduced for their retrieval. Our model was indeed only "un-fine-tuned" with respect to the quantitative fitting of static FC and modified to generate some unspecific kind of switching FC non-stationarity, which was qualitatively reminiscent of empirical observations. For this reason, our model is unfit to provide estimates of the actual number of FC states. In our study, clusters of related FC(t) matrices were extracted via a rough unsupervised clustering procedure. However, the parameters of the clustering algorithm were not finely optimized, but only selected to allow a proper segmentation of the visually prominent 'blocks' of metastable FC patterns in the empirical and simulated FCD matrices.

For this same reason, our model is currently under-constrained so that extrapolations based on it could be quantitatively unreliable. As discussed earlier in the present study, fitting a unique static FC matrix appears to be a misleading direction, since the parameters with the closest correspondence to static empirical FC lead to trivial FCD matrices. Neglecting FC dynamics might also account for a large fraction of the unexplained variability of static FC and the poor predictability as observed in experimental studies (Müller et al., 2013). In order to be genuinely predictive, future whole brain dynamical models should be fine tuned to best fit an entire target set of typical FC states, as well as the associated state-to-state transition probabilities (Allen et al., 2012), reflected in characteristic ensembles of FCD matrices, which could be sampled over empirical BOLD recordings. A larger analysis effort will be required to gather the necessary information about FC states features and statistics in actual resting state data, in control as well as pathological conditions. The available information is indeed currently still very limited and is potentially flawed by the widespread application of pre-processing steps, such as global regression, which could interact in an uncontrolled manner (Saad et al., 2012) with non-stationary changes of FC related to global brain state switching.

Nonetheless, at the qualitative level, our model provides an insight into the nature of FC states. Naturally free from physiological artifacts —such as e.g. respiratory variation (Birn et al., 2006)—, mean field simulations may become a fundamental tool for linking observed patterns of non-stationary switching between FC states with aspects of the underlying neural dynamics, constrained by an imposed SC. We expect that whole brain simulations will simultaneously be able to emulate different imaging modalities (as in the case of "The Virtual Brain" simulator (Sanz Leon et al., 2013), casting light on the links existing between BOLD FC states and the faster dynamics of EEG/MEG microstates (Mantini et al., 2007; Van De Ville et al., 2010) across different temporal and spatial scales.

Retrieving a mapping from imaged FC states to actual (hidden) states of brain activity and their evolution will facilitate the formulation of hypotheses about the role played in cognition by the switching between different FC states, by assessing modulations linked to state switching of the way, in which brain regions share information (Battaglia et al., 2012).

Finally, model-driven explorations could be used to investigate how modifications of SC or the working point of brain dynamics (Deco et al., 2013b) translate into aberrant FC non-stationarity patterns as in Schizophrenia (Sakoglu et al., 2010) and Alzheimer's disease (Jones et al., 2012). These disorders —together with ageing (Ferreira and Busatto,

2013)— may not necessarily be characterized by alterations in individual FC states (captured by FC(t) matrices) but rather by the statistics of visiting times and inter-state transitions (captured by FCD matrices). We thus foresee that dynamical, beyond static (Menon, 2011), FC studies will be able to inspire novel disease biomarkers for the diagnosis, prognosis and personalization of treatment.

Supplementary data to this article can be found online at http://dx.doi.org/10.1016/j.neuroimage.2014.11.001.

Acknowledgments

The research reported herein was supported by the Brain Network Recovery Group through the James S. McDonnell Foundation and funding from the European Union Seventh Framework Programme (FP7-ICT BrainScales and Human Brain Project (grant no. 60402)). DB was supported by the Marie Curie career development fellowship FP7-IEF 330792 (DynViB) and by the Federal Ministry of Education and Research (BMBF) Germany under grant number 01GQ1005B. We thank Patrick Hagmann and his group for providing the empirical data.

References

Allen, E.A., Damaraju, E., Plis, S.M., Erhardt, E.B., Eichele, T., Calhoun, V.D., 2012. Tracking whole-brain connectivity dynamics in the resting state. Cereb. Cortex. http://dx.doi.org/10.1093/cercor/bhs352.

Battaglia, D., Witt, A., Wolf, F., Geisel, T., 2012. Dynamic effective connectivity of inter-areal brain circuits. PLoS Comput. Biol. 8, e1002438.

Beggs, J., Plenz, D., 2003. Neuronal avalanches in neocortical circuits. J. Neurosci. 23, 11167–11177.

Birn, R.M., Diamond, J.B., Smith, M.A., Bandettini, P.A., 2006. Separating respiratory-variation-related fluctuations from neuronal-activity-related fluctuations in fMRI. NeuroImage 31, 1536–1548.

Bressler, S.L., Kelso, J.A.S., 2001. Cortical coordination dynamics and cognition. Trends Cogn. Sci. 5, 26–36.

Britz, J., Van De Ville, D., Michel, C.M., 2010. BOLD correlates of EEG topography reveal rapid resting-state network dynamics. NeuroImage 52, 1162–1170.

Cabral, J., Hugues, E., Sporns, O., Deco, G., 2011. Role of local network oscillations in resting-state functional connectivity. NeuroImage 57, 130–139.

Damoiseaux, J.S., Greicius, M.D., 2009. Greater than the sum of its parts: a review of studies combining structural connectivity and resting-state functional connectivity. Brain Struct. Funct. 213, 525–533.

Damoiseaux, J.S., Rombouts, S., Barkhof, F., Scheltens, P., Stam, C.J., Smith, S.M., Beckmann, C.F., 2006. Consistent resting-state networks across healthy subjects. Proc. Natl. Acad. Sci. U. S. A. 103, 13848–13853.

Deco, G., Jirsa, V.K., 2012. Ongoing cortical activity at rest: criticality, multistability, and ghost attractors. J. Neurosci. 32, 3366–3375.

Deco, G., Jirsa, V., McIntosh, A.R., Sporns, O., Kötter, R., 2009. Key role of coupling, delay, and noise in resting brain fluctuations. Proc. Natl. Acad. Sci. U. S. A. 106, 10302–10307.

Deco, G., Jirsa, V.K., Mcintosh, A.R., 2011. Emerging concepts for the dynamical organization of resting-state activity in the brain. Nat. Rev. Neurosci. 12, 43–56.

Deco, G., Senden, M., Jirsa, V., 2012. How anatomy shapes dynamics: a semi-analytical study of the brain at rest by a simple spin model. Front. Comput. Neurosci. 6, 68.

Deco, G., Ponce-Alvarez, A., Mantini, D., Romani, G.L., Hagmann, P., Corbetta, M., 2013a. Resting-state functional connectivity emerges from structurally and dynamically shaped slow linear fluctuations. J. Neurosci. 33 (27), 11239–11252.

Deco, G., Jirsa, V.K., Mcintosh, A.R., 2013b. Resting brains never rest: computational insights into potential cognitive architectures. Trends Neurosci. 36, 268–274.

Desikan, R.S., Ségonne, F., Fischl, B., Quinn, B.T., Dickerson, B.C., Blacker, D., Buckner, R.L., Dale, A.M., Maguire, R.P., Hyman, B.T., Albert, M.S., Killiany, R.J., 2006. An automated labeling system for subdividing the human cerebral cortex on MRI scans into gyral based regions of interest. NeuroImage 31 (3), 968–980.

Doucet, G., Naveau, M., Petit, L., Zago, L., Crivello, F., Jobard, G., Delcroix, N., Mellet, E., Tzourio-Mazoyer, N., Mazoyer, B., Joliot, M., 2012. Patterns of hemodynamic low-frequency oscillations in the brain are modulated by the nature of free thought during rest. NeuroImage 59, 3194–3200.

Ferreira, L.K., Busatto, G.F., 2013. Resting-state functional connectivity in normal brain aging. Neurosci. Biobehav. Rev. 37 (3), 384–400.

Friston, K.J., 2011. Functional and effective connectivity: a review. Brain Connect. 1, 13–36.

Friston, K.J., Harrison, L., Penny, W., 2003. Dynamic causal modelling. NeuroImage 19, 1273–1302.

Galan, R.F., 2008. On how network architecture determines the dominant patterns of spontaneous neural activity. PLoS ONE 3, e2148.

Ghosh, A., Rho, Y., McIntosh, A.R., Kötter, R., Jirsa, V.K., 2008. Noise during rest enables the exploration of the brain's dynamic repertoire. PLoS Comp. Biol. 4, e1000196.

Goñi, J., van den Heuvel, M.P., Avena-Koenigsberger, A., Velez, N., de Mendizabal, R.F., Betzel, A. Griffa, Hagmann, P., Corominas-Murtra, B., Thiran, J.P., Sporns, O., 2014. Resting-brain functional connectivity predicted by analytic measures of network communication. Proc. Natl. Acad. Sci. U. S. A. 111, 833–838.

Gusnard, D.A., Raichle, M.E., 2001. Searching for a baseline: functional imaging and the resting human brain. Nat. Rev. Neurosci. 2, 685–694.

Hagmann, P., Cammoun, L., Gigandet, X., Meuli, R., Honey, C.J., Wedeen, V.J., Sporns, O., 2008. Mapping the structural core of human cerebral cortex. PLoS Biol. 6, e159.

Hartigan, J.A., Wong, M.A., 1979. Algorithm AS 136: a K-means clustering algorithm. J. R. Stat. Soc.: Ser. C: Appl. Stat. 28, 100–108.

Honey, C.J., Kötter, R., Breakspear, M., Sporns, O., 2007. Network structure of cerebral cortex shapes functional connectivity on multiple time scales. Proc. Natl. Acad. Sci. U. S. A. 104, 10240–10245.

Horsthemke, W., Lefever, R., 2006. Noise-induced transitions. Springer, Berlin Heidelberg.

Hutchison, R.M., Womelsdorf, T., Allen, E.A., Bandettini, P.A., Calhoun, V.D., Corbetta, M., Della Penna, S., Duyn, J., Glover, G., Gonzalez-Castillo, J., Handwerker, D.A., Keilholz, S., Kiviniemi, V., Leopold, D.A., de Pasquale, F., Sporns, O., Walter, M., Chang, C., 2013. Dynamic functional connectivity: promise, issues, and interpretations. NeuroImage 80, 360–378.

Jones, D.T., Vemuri, P., Murphy, M.C., Gunter, J.L., Senjem, M.L., Machulda, M.M., Przybelski, S.A., Gregg, B.E., Kantarci, K., Knopman, D.S., Boeve, B.F., Petersen, R.C., Jack Jr., C.R., 2012. Non-stationarity in the "resting brain's" modular architecture. PLoS ONE 7, e39731.

Laird, A.R., Fox, P.M., Eickhoff, S.B., Turner, J.A., Ray, K.L., McKay, D.R., Glahn, D.C., Beckmann, C.F., Smith, S.M., Fox, P.T., 2011. Behavioral interpretations of intrinsic connectivity networks. J. Cogn. Neurosci. 23, 4022–4037.

Liu, X., Duyn, J.H., 2013. Time-varying functional network information extracted from brief instances of spontaneous brain activity. Proc. Natl. Acad. Sci. U. S. A. 110, 4392–4397.

Mannella, R., 2002. Integration of stochastic differential equations on a computer. Int. J. Mod. Phys. C 13, 1177–1194.

Mantini, D., Perrucci, M.G., Del Gratta, C., Romani, G.L., Corbetta, M., 2007. Electrophysiological signatures of resting state networks in the human brain. Proc. Natl. Acad. Sci. U. S. A. 104, 13170–13175.

Manuca, R., Savit, R., 1996. Stationarity and nonstationarity in time series analysis. Physica D 99, 134–161.

Menon, V., 2011. Large-scale brain networks and psychopathology: a unifying triple network model. Trends Cogn. Sci. 15, 483–506.

Messé, A., Rudrauf, D., Benali, H., Marrelec, G., 2014. Relating structure and function in the human brain: relative contributions of anatomy, stationary Dynamics, and non-stationarities. PLoS Comp. Biol. 10, e1003530.

Miller, P., Brody, C.D., Romo, R., Wang, X.-J., 2003. A recurrent network model of somatosensory parametric working memory in the prefrontal cortex. Cereb. Cortex 13, 1208–1218.

Moretti, P., Muñoz, M.A., 2013. Griffiths phases and the stretching of criticality in brain networks. Nat. Commun. 4, 2521.

Müller, S., Wang, D., Fox, M.D., Yeo, B.T., Sepulcre, J., Sabuncu, M.R., Shafee, R., Lu, J., Liu, H., 2013. Individual variability in functional connectivity architecture of the human brain. Neuron 77, 586–595.

Rabinovich, M., Huerta, R., Laurent, G., 2008. Transient dynamics for neural processing. Science 321, 48–50.

Raichle, M.E., Mintun, M.A., 2006. Brain work and brain imaging. Annu. Rev. Neurosci. 29, 449–476.

Rubinov, M., Sporns, O., 2010. Complex network measures of brain connectivity: uses and interpretations. NeuroImage 52 (3), 1059–1069.

Saad, Z.S., Gotts, S.J., Murphy, K., Chen, G., Jo, H.J., Martin, A., Cox, R.W., 2012. Trouble at Rest: How Correlation Patterns and Group Differences Become Distorted After Global Signal Regression. Brain Connect. 2, 25–32.

Sakoglu, U., Pearlson, G.D., Kiehl, K.A., Wang, Y., Michael, A., Calhoun, V.D., 2010. A method for evaluating dynamic functional network connectivity and task-modulation: application to schizophrenia. MAGMA 23, 351–366.

Sanz Leon, P., Knock, S.A., Woodman, M.M., Domide, L., Mersmann, J., McIntosh, A.R., Jirsa, V., 2013. The Virtual Brain: a simulator of primate brain network dynamics. Front. Neuroinform. 7, 10.

Van De Ville, D., Britz, J., Michel, C.M., 2010. EEG microstate sequences in healthy humans at rest reveal scale-free dynamics. Proc. Natl. Acad. Sci. U. S. A. 107, 18179–18184.

Wong, K.F., Wang, X.J., 2006. A recurrent network mechanism of time integration in perceptual decisions. J. Neurosci. 26, 1314–1328.